RAPID COMMUNICATION

Far-field tectonic effects of the Arabia–Eurasia collision and the inception of the North Anatolian Fault system

IRENE ALBINO*, WILLIAM CAVAZZA*†, MASSIMILIANO ZATTIN‡,
ARAL I. OKAY§, SHOTA ADAMIA¶ & NINO SADRADZE‖

*Department of Biological, Geological and Environmental Sciences, University of Bologna,
Piazza di Porta San Donato 1, 40126 Bologna, Italy
‡Department of Geosciences, University of Padua, Via Gradenigo 6, 35131 Padua, Italy
§Istanbul Technical University, Eurasia Institute of Earth Sciences, Maslak 34469, Istanbul, Turkey
¶Institute of Geophysics, 1 M. Alexidze str., 0193 Tbilisi, Georgia
‖Geological Institute, 1/9 M. Alexidze str., 0193 Tbilisi, Georgia

Abstract

New thermochronological data show that rapid Middle Miocene exhumation occurred synchronously along the Bitlis suture zone and in the southeastern Black Sea region, arguably as a far-field effect of the Arabia–Eurasia indentation. Collision-related strain focused preferentially along the rheological boundary between the multideformed continental lithosphere of northeastern Anatolia and the strong (quasi)oceanic lithosphere of the eastern Black Sea. Deformation in the southeastern Black Sea region ceased in late Middle Miocene time, when coherent westward motion of Anatolia and the corresponding activation of the North and East Anatolian Fault systems mechanically decoupled portions of the foreland from the Arabia–Eurasia collision zone.

Keywords: fission-track analysis, low-temperature thermochronology, stress transfer, exhumation.

1. Introduction

The Bitlis–Zagros orogenic belt of western Asia and the related wide area of deformation within the European foreland to the north (Fig. 1) are regarded as one of the best examples of ongoing continental collision in the world. Present-day reduction of surface area within the collision zone is estimated at 31×10^3 km^2 Ma^{-1} (Reilinger *et al.* 2006). Most of the decrease in surface area is being accommodated by coherent lateral transport of Anatolia out of the collision zone (*c.* 70 %) and by shortening along the Bitlis–Zagros and Greater Caucasus orogenic wedges (*c.* 15 %). The remaining decrease in surface area is distributed across the Anatolian–Iranian plateau and the Lesser Caucasus (Fig. 2).

The age of the initial collision between Arabia and Eurasia has been the topic of much debate, with estimates of Late Cretaceous (Hall, 1976; Berberian & King, 1981; Alavi, 1994), Late Eocene – Oligocene (35–25 Ma, Jolivet & Faccenna, 2000; Agard *et al.* 2005; Vincent *et al.* 2007; Allen & Armstrong, 2008), Miocene (Şengör, Görür & Şaroğlu, 1985; Dewey *et al.* 1989; Yılmaz, 1993; Robertson *et al.*

†Author for correspondence: william.cavazza@unibo.it

2007) and Pliocene (Philip *et al.* 1989; Avdeev & Niemi, 2011). The only available low-temperature thermochronological dataset for the Bitlis collision front points to an episode of fast exhumation in the Middle Miocene (Okay, Zattin & Cavazza, 2010), in agreement with the stratigraphy of the adjacent foreland basins.

In this paper, the first low-temperature thermochronological dataset for the Eurasian foreland north of the Bitlis collision zone suggests that the tectonic stresses related to the Arabian indentation were transmitted efficiently over large distances, focusing preferentially at rheological discontinuities along the eastern Black Sea coast and in the Lesser Caucasus. Since the late Middle Miocene a new tectonic regime has been active, as the westward translation of Anatolia (e.g. McKenzie, 1972; Dewey & Şengör, 1979; Şengör, 1979; Şengör *et al.* 2005) is accommodating most of the Arabia–Eurasia convergence, thus precluding efficient northward stress transfer.

2. Geological setting

The study area represents the region of maximum indentation between Arabia and Eurasia (Fig. 1). From north to south, four major geological provinces are present: (i) the eastern Black Sea (EBS), (ii) the eastern Pontides (EP) portion of the Sakarya Zone, (iii) the Anatolide–Tauride block (ATB), and (iv) the Arabian platform (AP).

(i) The more than 2000 m deep EBS is partly floored by quasi-oceanic crust and represents the remnant of a composite Paleocene – Middle Eocene back-arc basin, which developed on the Eurasian upper plate during N-dipping subduction of the Neotethys (e.g. Spadini, Robinson & Cloetingh, 1997; Stampfli & Borel, 2004; Edwards *et al.* 2009).

(ii) The EP are the easternmost segment of a W–E-trending composite mountain belt traceable for more than 1200 km from Thrace to the Adjara–Trialeti region of the Lesser Caucasus of Georgia (Fig. 1). The EP are part of the Sakarya Zone, a continental fragment of Laurasian affinity (Okay & Tüysüz, 1999; Cavazza *et al.* 2012).

(iii) The ATB forms the bulk of southern Turkey (Fig. 1) and can be traced to the east in Transcaucasia and Iran. In contrast to the Pontides, the ATB shows a stratigraphy similar to the AP (Okay & Tüysüz, 1999). The Palaeogene
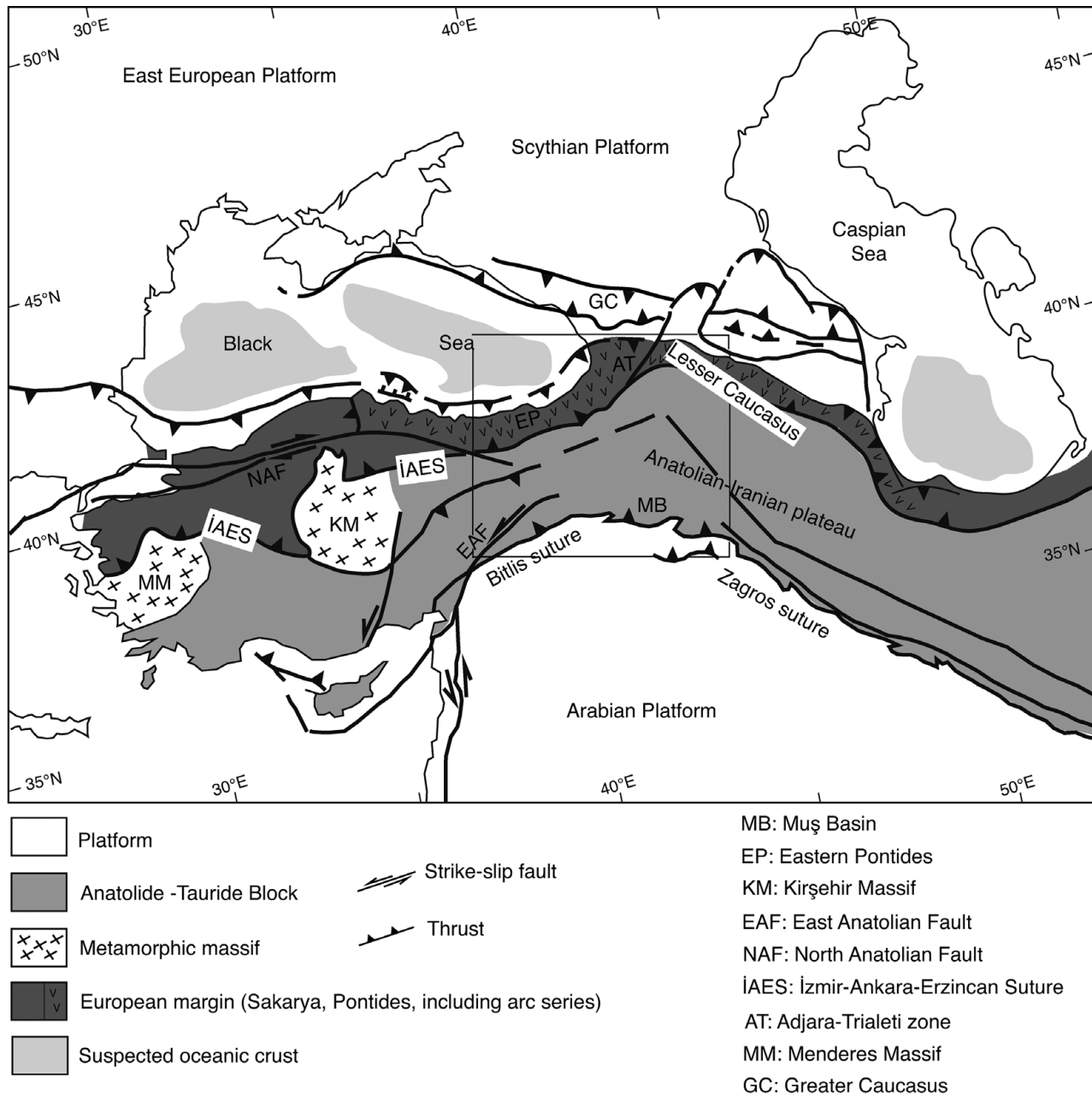
Figure 1. Tectonic map of Asia Minor and Transcaucasia (modified from Sosson *et al.* 2010).

İzmir–Ankara–Erzincan suture marks the boundary between the ATB and the Sakarya Zone to the north.

(iv) The southern portion of the study area is characterized by the Gondwanian terranes of the AP flexurally bent towards the Bitlis–Zagros orogenic front to the north.

3. Apatite fission-track data and thermal modelling

We collected samples for apatite fission-track (AFT) analysis across a wide swath of territory from the EP and Adjara–Trialeti region to the north to the Bitlis collision zone to the south. The samples were taken from a variety or rock types, comprising Cretaceous and Palaeogene granitoids, gneisses and metasandstone of the Bitlis and Pütürge massifs, and deeply buried Palaeogene sandstones (Table 1). Very few localities were suitable for sampling in the eastern Anatolian Plateau since most of this region is covered by a thick

pile of Plio-Quaternary volcanic and volcaniclastic rocks. Procedures for sample preparation and analysis are those described in Zattin *et al.* (2000). Apatite grains from 60 samples were sent for irradiation. However, only 26 samples yielded apatite grains suitable for fission-track analysis.

Despite the lithological and age diversity, AFT results have a consistent geographic distribution, with younger ages (18–12 Ma; Early–Middle Miocene) in the Bitlis orogen and in the easternmost Pontides along the Black Sea, and Palaeogene ages in the Anatolian Plateau and Adjara–Trialeti region (Table 1; Fig. 3). There is no relationship between AFT ages and sample elevations.

Modelling on samples containing a statistically significant number of confined tracks constrained further the thermochronological evolution of the study area (Fig. 4). Sample TU274 (Late Cretaceous granodioritic body of the EP magmatic arc) shows a phase of fast cooling (average cooling rate *c.* 22 °C Ma^{-1}) between *c.* 16 and 14 Ma. Considering

Table 1. Apatite fission-track data

Sample number	Coordinates (UTM)	Elevation (m)	Rock type	Age	No. of crystals	Spontaneous		Induced		$P(\chi^2)$	Dosimeter		FT Age (Ma) $\pm 1\sigma$	MCTL (μm) $\pm$ std. err.	Std. dev.	Tracks measured
						ρ_s	N_s	ρ_i	N_i		ρ_d	N_d				
TU250	37S 0676940 4368287	1933	Sandstone	Eocene	20	2.10	107	1.26	640	52.30	1.41	4679	40.5 ± 5.2	-	-	-
TU253	37S 0732079 4344155	1652	Sandstone	Paleocene	9	1.36	33	0.94	227	70.39	1.42	4237	35.9 ± 6.9	12.72 ± 0.12	1.84	13
TU254	37S 0754492 4344155	1458	Sandstone	Oligocene	6	1.31	35	0.73	194	59.76	1.40	4798	37.8 ± 10.7	-	-	-
TU255	37S 0750864 4293994	1339	Sandstone	Oligocene	17	1.98	122	0.65	481	87.12	1.43	4679	53.3 ± 1.7	13.85 ± 0.20	1.29	35
TU256	38S 0382766 4246434	1948	Sandstone	Oligocene	17	1.23	25	0.43	141	53.02	1.50	4376	44.6 ± 10.0	-	-	-
TU260	38S 0361398 4337228	1743	Sandstone	Oligocene	22	2.28	39	1.20	204	95.57	1.40	4659	44.8 ± 8.1	-	-	-
TU264	38S 0370895 4384757	1862	Granite	Late Cretaceous	15	3.74	134	3.62	1295	100.00	1.50	4736	26.0 ± 2.7	14.48 ± 0.19	1.04	50
TU266	38T 0330734 4454167	1401	Sandstone	Eocene	20	2.21	129	3.43	1196	80.32	1.50	4568	25.0 ± 2.8	13.60 ± 0.14	0.70	8
TU267	38T 0662375 4513739	1086	Metadiorite	Hercynian	20	2.80	189	1.46	982	57.37	1.40	4978	44.4 ± 3.0	-	-	-
TU273	37T 0743625 4761028	842	Granite	Late Cretaceous	18	2.26	179	1.63	1134	98.10	1.40	4823	12.4 ± 2.6	11.91 ± 0.28	0.93	5
TU274	37T 0743625 4761028	952	Granodiorite	Late Cretaceous	20	2.17	137	3.53	2226	86.66	1.33	4536	13.4 ± 1.4	14.57 ± 0.15	1.38	37
TU275	37T 0681167 4494619	1055	Granite	Eocene	20	1.65	51	1.43	662	80.24	1.40	4890	12.2 ± 2.7	12.61 ± 0.12	1.97	11
TU276	37T 0665263 4481103	1256	Granite	Eocene (?)	15	1.79	62	2.03	702	98.38	1.40	4653	20.7 ± 2.9	11.36 ± 0.13	1.39	5
TU278	38T 0374158 4658977	867	Granite	Paleocene	14	2.17	36	1.03	879	50.30	1.40	4459	46.9 ± 5.2	-	-	-
TU279	38T 0260294 4641212	334	Granodiorite	Eocene	17	4.99	262	3.27	1716	95.52	1.30	4438	33.1 ± 2.7	13.41 ± 0.12	1.43	50
TU281	37T 0747431 4607962	376	Diorite	Late Eocene (?)	8	1.73	37	1.91	409	99.19	1.00	4298	15.2 ± 2.7	-	-	-
TU282	38T 0368846 4636796	813	Flysch	Paleocene	14	1.34	76	0.70	197	58.30	1.40	4432	37.5 ± 5.6	-	-	-
TU284	38T 0444177 4570059	1047	Granite	Late Cretaceous	16	3.02	151	1.87	933	99.24	1.10	4765	29.2 ± 4.0	12.23 ± 0.22	0.48	21
TU285	38T 0445889 4568770	1187	Granite	Eocene (?)	20	4.82	375	3.48	2696	80.81	1.20	4678	23.3 ± 1.7	11.70 ± 0.12	1.29	6
TU136*	38S 0251160 4260508	1642	Metasandstone	Palaeozoic	20	0.72	40	0.89	496	100.00	0.90	4293	13.4 ± 2.2	13.98 ± 0.21	0.92	19
TU138*	38S 0241967 4249698	1285	Gneiss	Precambrian	16	0.46	22	0.55	264	100.00	0.90	4281	13.8 ± 3.1	-	-	-
TU140*	37S 0753971 4234870	871	Sandstone	Paleocene/Eocene	4	5.14	43	4.84	405	91.10	0.90	4256	17.5 ± 2.8	-	-	-
TU145*	37S 0630748 4277901	1175	Metagranite	Precambrian	20	0.55	38	0.62	425	82.50	0.89	4219	14.6 ± 2.5	-	-	-
TU149*	37S 0476619 4240707	1395	Gneiss	Eocene	20	1.60	112	1.44	1006	87.00	0.88	4181	18.0 ± 1.8	13.00	1.99	72
TU155*	38S 0321648 4195176	1607	Sandstone	Eocene	20	0.88	53	1.18	711	65.10	1.01	4818	13.9 ± 2.1	14.51 ± 0.29	1.41	24
TU159*	38S 0396240 4162747	1342	Sandstone	Eocene	6	0.53	14	0.39	102	75.40	1.00	4771	25.2 ± 7.2	-	-	-

MCTL – mean confined track length. Central ages calculated using dosimeter glass CN5 and ζ-CN5 = 336.34 ± 16.24 (analyst I. Albino). ρ_s – spontaneous track densities ($\times 10^5$ cm^{-2}) measured in internal mineral surfaces; N_s – total number of spontaneous tracks; ρ_i and ρ_d – induced and dosimeter track densities ($\times 10^6$ cm^{-2}) on external mica detectors ($g = 0.5$); N_i and N_d – total numbers of tracks; $P(\chi^2)$ – probability of obtaining χ^2-value for ν degrees of freedom (where ν = number of crystals − 1); a probability > 5 % is indicative of a homogenous population. Samples with a probability < 5 % have been analysed with the binomial peak-fitting method. (*) Ages from Okay, Zattin & Cavazza (2010) (analyst M. Zattin).
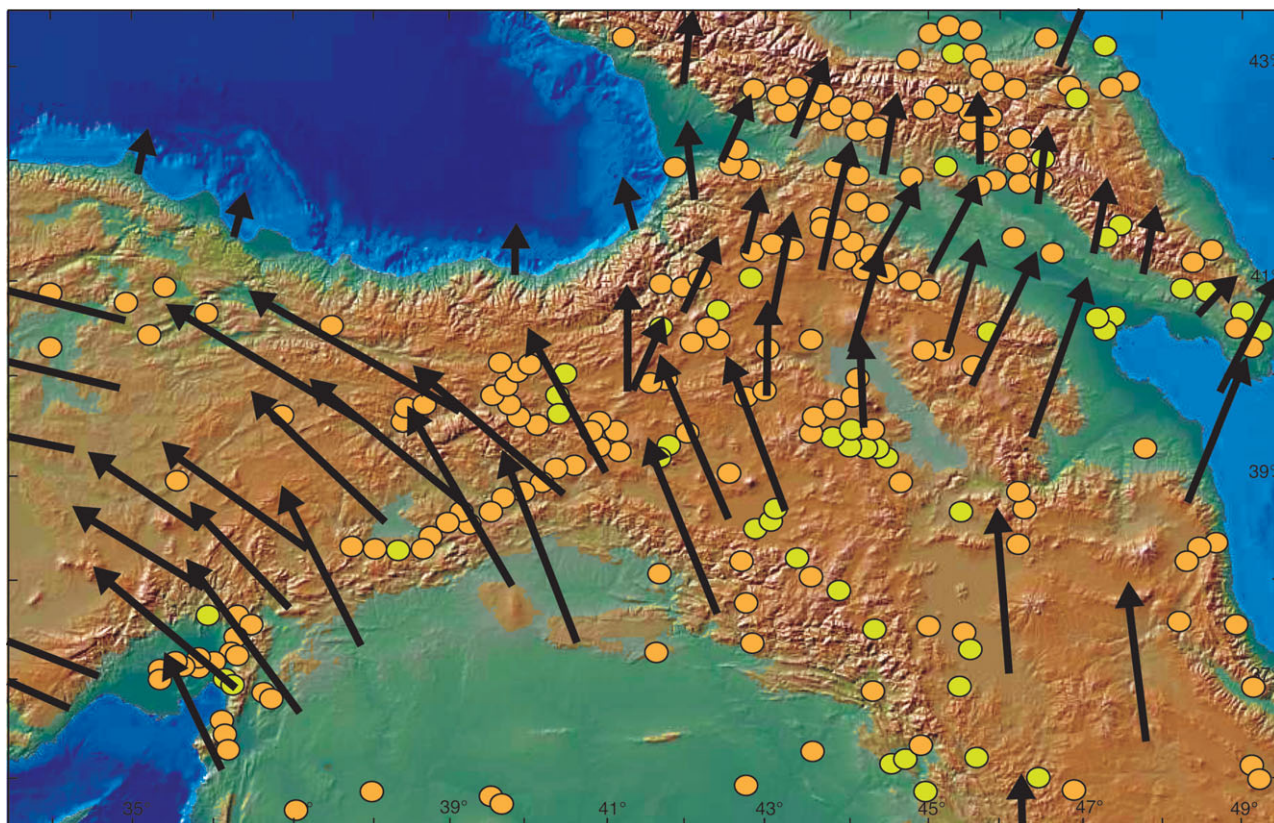
Figure 2. Digital elevation model of the Eastern Mediterranean and the Middle East. The arrows indicate the GPS-derived velocities with respect to a stationary Eurasia (modified from Reilinger *et al.* 2006; Copley & Jackson, 2006); the dots indicate the epicentres of earthquakes M > 4.8 (depth of hypocentres: orange dots 0–33 km; yellow dots: 33–70 km) (1973–2012 data from USGS/NEIC PDE online catalogue).

a geothermal gradient of 25–30 °C km^{-1}, based on heat flow (Tezcan, 1995), the average exhumation rate in the easternmost Pontides during this period of cooling is 0.7–0.9 km Ma^{-1}. Cooling/exhumation in the EP mirrors the evolution of the Bitlis–Pütürge massif along the Arabia–Eurasia collision zone where sample TU149 (Pan-African augen gneiss) shows a rapid increase in exhumation at *c.* 12 Ma (Fig. 4; see also Okay, Zattin & Cavazza, 2010, p. 37).

Sample TU255 is an early Oligocene sandstone turbidite at the base of the Muş basin, a foreland basin located north of the Bitlis suture and associated with northward subduction of the Arabian plate (Hüsing *et al.* 2009). Following deposition, this sample was progressively buried and entered the apatite partial annealing zone (PAZ) at about 23 Ma. A rapid phase of cooling/exhumation began at 19 Ma (late Early Miocene), likely the result of the progressive incorporation of the basin southern margin into the growing Bitlis orogenic wedge. Post-depositional burial of sample TU255 was not deep enough to completely erase the thermochronological record of the sediment source rocks, showing a Late Cretaceous – Palaeogene episode of cooling/exhumation correlatable with widespread deformation in the area related to the closure of the İzmir–Ankara–Erzincan ocean (Okay & Tüysüz, 1999).

Sample TU279 (Eocene granodiorite intruding volcanic/volcaniclastic rocks in the Adjara–Trialeti zone of western Georgia) shows very rapid cooling at 36–35 Ma (latest Eocene), in line with thermochronological data from the western Greater Caucasus (Vincent *et al.* 2011). The sample then underwent progressive heating during most of the Miocene and cooled definitively outside the apatite

PAZ (120–60 °C) in the Late Miocene, likely the result of orogenic-wedge dynamics in the Adjara–Trialeti northward-verging nappe stack facing the flexural foreland basin to the north.

4. Discussion and conclusions

Our thermochronological dataset shows that exhumation of Cretaceous and Eocene granitoids along the easternmost Pontides occurred in the Middle Miocene. The notion of a discrete and relatively rapid mid-Miocene episode of exhumation/erosion in the region is also supported by unpublished fission-track data from the composite Kackar batholith (Cretaceous – Late Eocene) immediately west of our study area (R. Jonckheere, pers. comm., 2012). The previously unrecognized exhumation/erosion episode along the Black Sea coast documented here mirrors the age of maximum tectonic coupling between the Eurasian and Arabian plates along the 2400 km long Bitlis–Zagros suture zone, *c.* 250 km to the south: exhumation ages along the easternmost Pontides are virtually identical to those obtained by Okay, Zattin & Cavazza (2010) along the Bitlis suture. We argue that tectonic stresses generated along the Bitlis collision zone were transmitted northward across eastern Anatolia and focused at the rheological boundary between the Anatolian continental lithosphere and the (quasi)oceanic lithosphere of the Black Sea.

Mechanical coupling of a collisional orogen and its forelands can induce far-field tectonic stresses and significant compressional structures at distances > 1500 km from a collision front (e.g. Ziegler, Cloetingh & Van Wees, 1995;
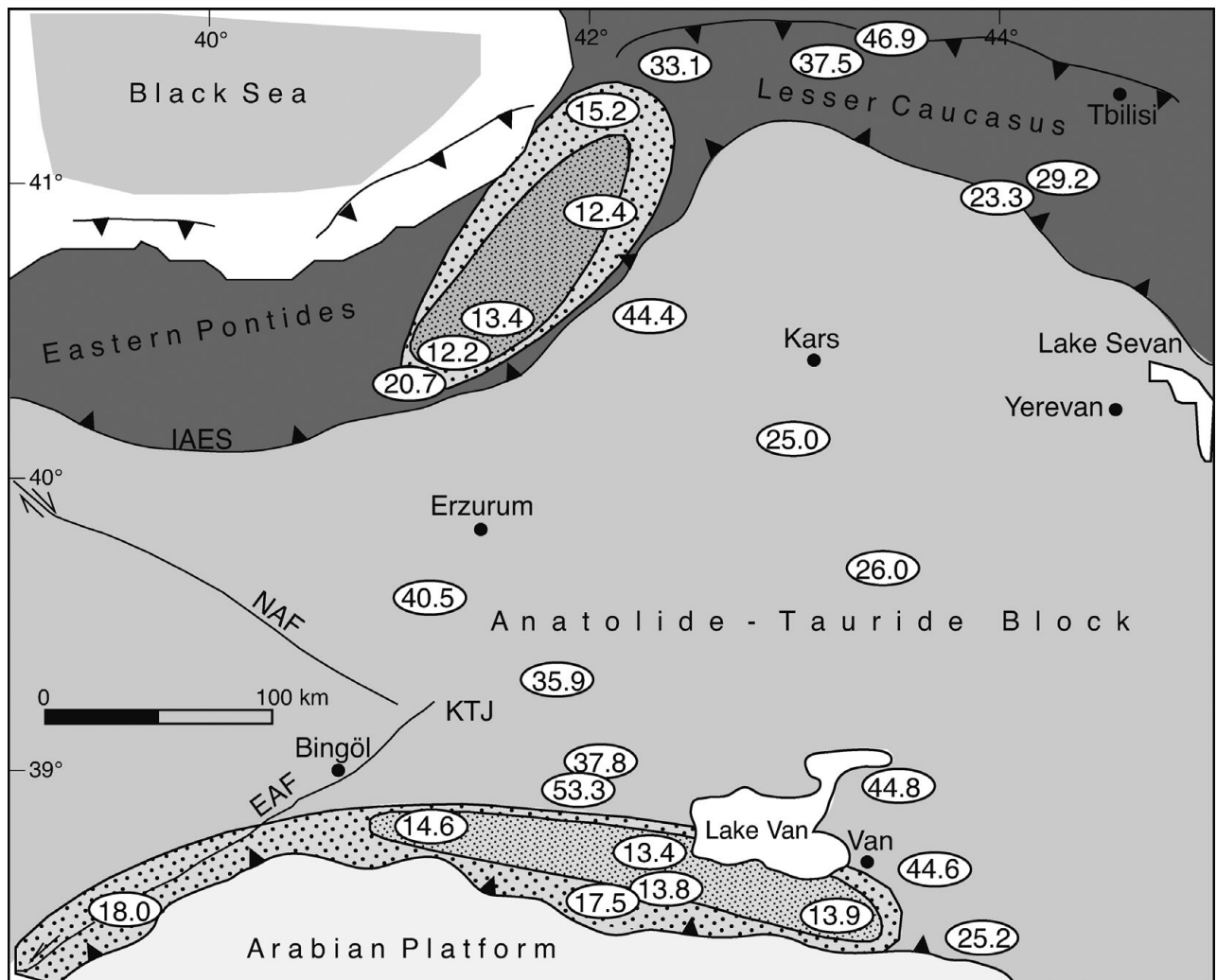
Figure 3. Geographic distribution of apatite fission-track ages. See Table 1 for complete dataset. The two dotted areas include all FT ages between *c.* 12–15 Ma and between *c.* 15–20 Ma. NAF – North Anatolian Fault; EAF – East Anatolian Fault; IAES – Izmir–Ankara–Erzincan suture; KTJ – Karliova triple junction.

Dickerson, 2003). Localization of compressional deformations far from the collision zone is controlled by spatial and temporal strength variations of the lithosphere (Ziegler, Van Wees & Cloetingh, 1998; Cloetingh *et al.* 2010). Passive continental margins – like the Black Sea coast of the study area – mark the largest compositional and rheological contrast within the lithosphere (Niu, O'Hara & Pearce, 2003) and are, therefore, preferential loci of deformation. Synchronous deformation at the opposing ends of the Anatolian continental plateau documented here mirrors the results of recent studies that argue for deformation at the northern margin of the Tibetan Plateau synchronous with the early stage of India–Asia collision (e.g. Yin *et al.* 2008; Clark *et al.* 2010). The area affected by faulting increased very little through time as the northern margin of Tibet was established early; deformation has propagated northward by only a minor amount during the entire period of collision. Dayem *et al.* (2009) showed that with certain boundary and initial conditions, thin viscous sheet calculations can yield significant strain rates in the northern part of Tibet soon after continental collision begins. Such conditions include (i) pre-existing topography in southern Tibet, (ii) short distances between India and northern Tibet at the time of collision, (iii) the presence of strong lithospheric blocks such as the Tarim Basin, and (iv)

pre-existing weaknesses in the Asian lithosphere. It is worth noting that several of these pre-conditions were met in our study area during the Arabia–Eurasia collision, as discussed in this section.

Cooling at temperatures below the apatite PAZ in the Anatolian Plateau and in the Lesser Caucasus (Adjara–Trialeti region of western Georgia) occurred instead in the Palaeogene (with a cluster of ages in the Middle – Late Eocene; Fig. 3; Table 1), coevally with the development of the İzmir–Ankara–Erzincan suture (e.g. Okay & Tüysüz, 1999). The successive uplift of the Anatolian Plateau did not exhume a new PAZ and thus is not recorded by the AFT data.

The GPS-derived velocity field for eastern Turkey, Transcaucasia and NW Iran (Fig. 2) shows that continental material north of the Bitlis suture appears to move around the oceanic lithosphere of the EBS. Vectors in eastern Anatolia point coherently to the west, defining the apparent 'extrusion' of the Anatolian plate, whereas east of the Karliova triple junction they show a progressive rotation to the east (McClusky *et al.* 2000; Reilinger *et al.* 2006). Similarly, the two areas are characterized by different deformation patterns. West of the triple junction the Anatolian plate is moving as a single entity bounded by the North and East Anatolian Fault systems, whereas east of it deformation is distributed along a
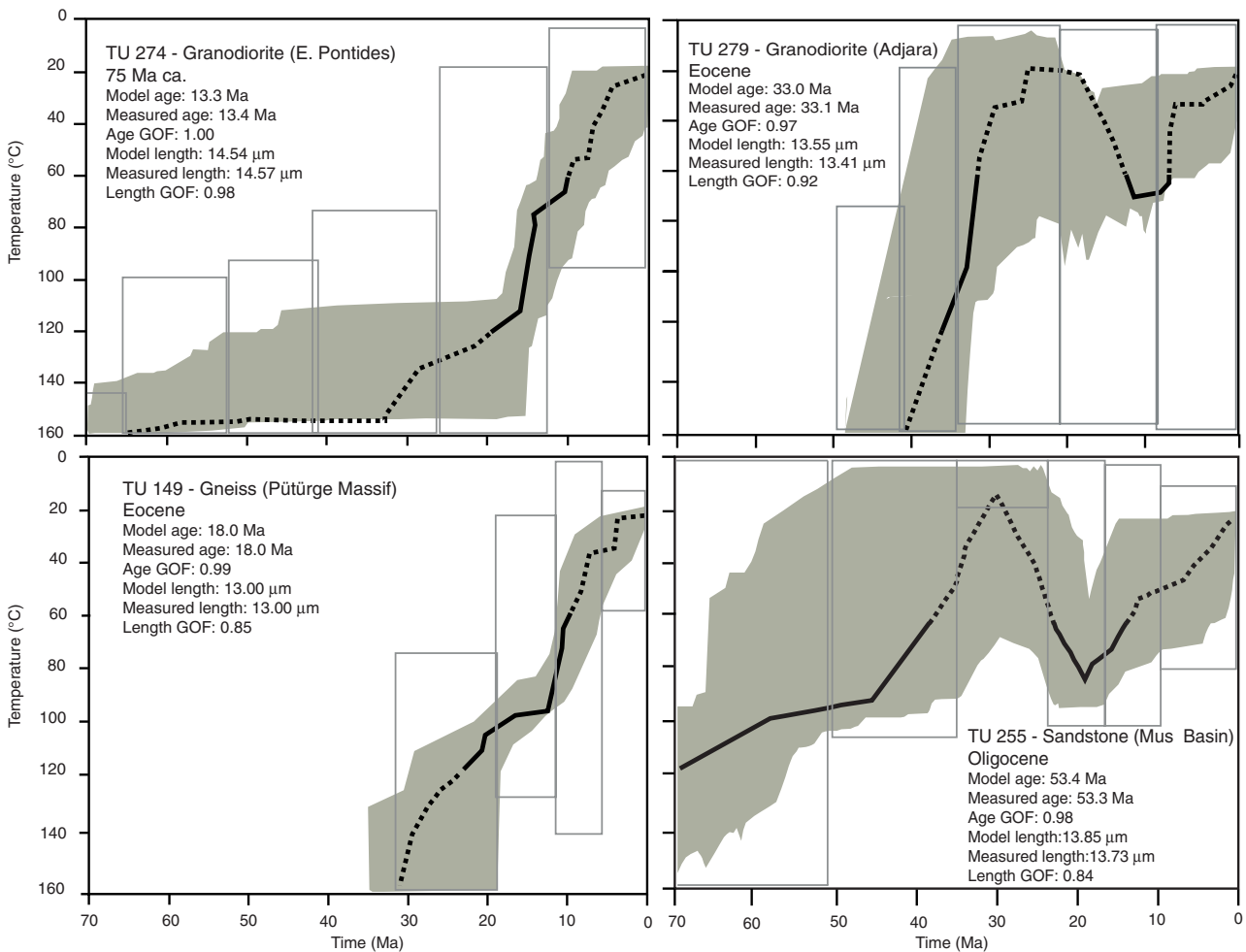
Figure 4. (Colour online) Time–temperature paths obtained from inverse modelling of AFT data using the HeFTy program (Ehlers *et al.* 2005), which generates the possible *T–t* paths by a Monte Carlo algorithm. Predicted AFT data were calculated according to the Ketcham, Donelick & Carlson (1999) annealing model and the Donelick, Ketcham & Carlson (1999) c-axis projection. Parameters (model and measured age, model and measured mean length) related to inverse modelling are reported. GOF (goodness-of-fit) values give an indication of the fit between observed and predicted data (values close to 1 are best). Shaded areas mark envelopes of statistically acceptable fit (GOF > 0.5) and the thick lines correspond to the most probable thermal histories. Thermal paths out of the partial annealing zone (dotted) are largely inferential as fission-track data cannot give reliable information out of this temperature range. Range and scale of *x*- and *y*-axes are identical in all diagrams to facilitate comparison.

complex system of strike-slip and thrust faults (Copley & Jackson, 2006; Adamia *et al.* 2011). The different deformation patterns can be explained by the different boundary conditions imposed on these two regions: westward motion of the Anatolian plate is favoured by slab retreat along the Hellenic trench (Jolivet, 2001) whereas eastern Turkey and Transcaucasia are caught between the Bitlis collision zone and the rheologically stronger (quasi)oceanic crust of the Black Sea to the northwest and the Eurasian continental crust to the northeast.

The analysis of present-day crustal dynamics and the thermochronological data presented in this paper provide a comparison between short- and long-term deformation patterns for the entire eastern Anatolian–Transcaucasian region. Two successive stages of Neogene deformation of the northwestern foreland of the Arabia–Eurasia collision zone can be inferred. (i) During the Early and Middle Miocene continental deformation was concentrated along the Arabia–Eurasia (Bitlis) collision zone but tectonic stress was transferred northward across eastern Anatolia, focusing along the EBS continent–ocean rheological transition. The Black Sea (quasi)oceanic lithosphere is fundamentally stronger than

the polydeformed continental lithosphere to the south and therefore represented a 'backstop' resisting deformation and deviating the impinging continental lithosphere (McClusky *et al.* 2000). (ii) Since late Middle Miocene time the westward translation of Anatolia and the activation of the North and East Anatolian Fault systems (Dewey & Şengör, 1979; Şengör, 1979; Şengör *et al.* 2005) have reduced efficient northward stress transfer. In this new tectonic regime – still active today – most of the Arabia–Eurasia convergence has been accommodated by the westward motion of Anatolia whereas the EP have been mechanically decoupled from the foreland of the Bitlis collision zone, as shown by the absence of significant seismicity in the area (Fig. 2). The following regional-scale topographic uplift of the Anatolian Plateau has not exhumed a new PAZ and thus is not recorded by the apatite fission tracks.

References

ADAMIA, S., ZAKARIADZE, G., CHKHOTUA, T., SADRADZE, N., TSERETELI, N., CHABUKIAN, A. & GVENTSADZE, A. 2011. Geology of the Caucasus: a review. *Turkish Journal of Earth Sciences* **20**, 489–544.

AGARD, P., OMRANI, J., JOLIVET, L. & MOUTHEREAU, F. 2005. Convergence history across Zagros (Iran): constraints from collisional an earlier deformation. *International Journal of Earth Sciences* **94**, 401–19.

ALAVI, M. 1994. Tectonics of the Zagros orogenic belt of Iran – new data and interpretations. *Tectonophysics* **229**, 211–38.

ALLEN, M. B. & ARMSTRONG, H. A. 2008. Arabia–Eurasia collision and the forcing of mid-Cenozoic global cooling. *Palaeogeography, Palaeoclimatology, Palaeoecology* **265**, 52–8.

AVDEEV, B. & NIEMI, N. A. 2011. Rapid Pliocene exhumation of the central Greater Caucasus constrained by low-temperature thermochronology. *Tectonics* **30**, TC2009, doi: 10.1029/2010TC002808.

BERBERIAN, M. & KING, G. 1981. Toward a paleogeography and tectonic evolution of Iran. *Canadian Journal of Earth Sciences* **18**, 210–65.

CAVAZZA, W., FEDERICI, I., OKAY, A. I. & ZATTIN, M. 2012. Apatite fission-track thermochronology of the Western Pontides (NW Turkey). *Geological Magazine* **149**, 133–40.

CLARK, M. K., FARLEY, K. A., ZHENG, D., WANG, Z. & DUVALL, A. R. 2010. Early Cenozoic faulting of the northern Tibetan Plateau margin from apatite (U–Th)/He ages. *Earth and Planetary Science Letters* **296**, 78–88.

CLOETINGH, S., VAN WEES, J. D., ZIEGLER, P. A., LENKEY, L., BEEKMAN, F., TESAURO, M., FÖRSTER, A., NORDEN, B., KABAN, M., HARDEBOL, N., BONTÉ, D., GENTER, A., GUILLOU-FROTTIER, L., Ter VOORDE, M., SOKOUTIS, D., WILLINGSHOFER, E., CORNU, T. & WORUM, G. 2010. Lithosphere tectonics and thermo-mechanical properties: an integrated modelling approach for Enhanced Geothermal Systems exploration in Europe. *Earth-Science Reviews* **102**, 159–206.

COPLEY, A. & JACKSON, J. 2006. Active tectonics of the Turkish-Iranian Plateau. *Tectonics* **25**, TC6006, doi: 10.1029/2005TC001906.

DAYEM, K. E., MOLNAR, P., CLARK, M. K. & HOUSEMAN, G. A. 2009. Far-field lithospheric deformation in Tibet during continental collision. *Tectonics* **28**, doi: 10.1029/2008TC002344.

DEWEY, J. F., HELMAN, M. L., TURCO, E., HUTTON, D. H. W. & KNOTT, S. D. 1989. Kinematics of the western Mediterranean. In *Alpine Tectonics* (eds M. P. Coward, D. Dietrich & R. G. Park), pp. 265–83. Geological Society of London, Special Publication no. 45.

DEWEY, J. F. & ŞENGOR, A. M. C. 1979. Aegean and surrounding regions: complex multiplate and continuum tectonics in a convergent zone. *Geological Society of America Bulletin* **90**, 84–92.

DICKERSON, P. W. 2003. Intraplate mountain building in response to continent-continent collision – the Ancestral Rocky Mountains (North America) and inferences drawn from the Tien Shan (Central Asia). *Tectonophysics* **365**, 129–42.

DONELICK, R. A., KETCHAM, R. A. & CARLSON, W. D. 1999. Variability of apatite fission-track annealing kinetics: II.

Crystallographic orientation effects. *American Mineralogist* **84**, 1224–34.

EDWARDS, R. A., SCOTT, C. L., SHILLINGTON, D. J., MINSHULL, T. A., BROWN, P. J. & WHITE, N. J. 2009. Wide-angle seismic data reveal sedimentary and crustal structure of the Eastern Black Sea. *The Leading Edge* **28**, 1056–65.

EHLERS, T. A., CHAUDHRI, T., KUMAR, S., FULLER, C. W., WILLETT, S. D., KETCHAM, R. A., BRANDON, M. T., BELTON, D. X., KOHN, B. P., GLEADOW, A. J. W., DUNAI, T. J. & FU, F. Q. 2005. Computational tools for low-temperature thermochronometer interpretation. *Reviews in Mineralogy & Geochemistry* **58**, 589–622.

HALL, R. 1976. Ophiolite emplacement and the evolution of the Taurus suture zone, southeastern Turkey. *Geological Society America Bulletin* **87**, 1078–88.

HÜSING, S. K., ZACHARIASSE, W. J., VAN HINSBERGEN, D. J. J., KRIJGSMAN, W., INCEÖZ, M., HARZHAUSER, M., MANDIC, O. & KROH, A. 2009. Oligo-Miocene foreland basin evolution in SE Anatolia: implications for the closure of the eastern Tethys gateway. In *Collision and Collapse at the Africa-Arabia-Eurasia Subduction Zone* (eds D.J.J. van Hinsbergen, M.A. Edwards & R. Govers), pp. 107–32. Geological Society of London, Special Publication no. 311.

JOLIVET, L. 2001. A comparison of geodetic and finite strain pattern in the Aegean, geodynamic implications. *Earth and Planetary Science Letters* **187**, 95–104.

JOLIVET, L. & FACCENNA, C. 2000. Mediterranean extension and the Africa-Eurasia collision. *Tectonics* **19**, 1095–106.

KETCHAM, R. A., DONELICK, R. A. & CARLSON, W. D. 1999. Variability of apatite fission-track annealing kinetics: III. Extrapolation to geological time scales. *American Mineralogist* **84**, 1235–55.

MCCLUSKY, S., BALASSANIAN, S., BARKA, A., DEMIR, C., ERGINTAV, S., GEORGIEV, I., GURKAN, M., HAMBURGER, K., HURST, H., KAHLE, K., KASTENS, G., KEKELIDZE, G., KING, R., KOTZEV, V., LENK, O., MAHMOUD, S., MISHIN, A., NADARIYA, M., OUZOUNIS, A., PARADISSIS, D., PETER, Y., PRILEPIN, M., REILINGER, R., SANLI, I., SEEGER, H., TEALEB, A., TOKSÖZ, M. N. & VEIS, G. 2000. Global Positioning System constraints on plate kinematics and dynamics in the eastern Mediterranean and Caucasus. *Journal of Geophysical Research* **105**, 5695–719.

MCKENZIE, D. 1972. Active tectonics of the Mediterranean region. *Geophysical Journal of the Royal Astronomical Society* **30**, 109–85.

NIU, Y., O'HARA, M. J. & PEARCE, J. A. 2003. Initiation of subduction zones as a consequence of lateral compositional buoyancy contrast within the lithosphere: a petrological perspective. *Journal of Petrology* **44**, 851–66.

OKAY, A. I. & TÜYSÜZ, O. 1999. Tethyan sutures of northern Turkey. In *The Mediterranean Basins: Tertiary Extension within the Alpine Orogen* (eds B. Durand, L. Jolivet, F. Horváth & M. Séranne), pp. 475–515. Geological Society of London, Special Publication no. 156.

OKAY, A. I., ZATTIN, M. & CAVAZZA, W. 2010. Apatite fission-track data for the Miocene Arabia-Eurasia collision. *Geology* **38**, 35–8.

PHILIP, H., CISTERNAS, A., GVISHIANI, A. & GORSHKOV, A. 1989. The Caucasus: an actual example of the initial stages of continental collision. *Tectonophysics* **161**, 1–21.

REILINGER, R., MCCLUSKY, S., VERNANT, P., LAWRENCE, S., ERGINTAV, S., CAKMAK, R., OZENER, H., KADIROV, F.,

GULIEV, I., STEPANYAN, R., NADARIYA, M., HAHUBIA, G., MAHMOUD, S., SAKR, K., ARRAJEHI, A., PARADISSIS, D., AL-AYDRUS, A., PRILEPIN, M., GUSEVA, T., EVREN, E., DMITROTSA, A., FILIKOV, S. V., GOMEZ, F., AL-GHAZZI, R. & KARAM, G. 2006. GPS constraints on continental deformation in the Africa-Arabia-Eurasia continental collision zone and implications for the dynamics of plate interactions. *Journal of Geophysical Research* **111**, B05411, doi: 10.1029/2005JB004051.

ROBERTSON, A. H. F., PARLAK, O., RIZAOĞLU, T., ÜNLÜGENÇ, Ü., İNAN, N., TASLI, K. & USTAÖMER, T. 2007. Tectonic evolution of the South Tethyan ocean: evidence from the Eastern Taurus Mountains (Elazığ region, SE Turkey). In *Deformation of Continental Crust* (eds A. C. Ries, R. W. H. Butler & R. H. Graham), pp. 231–70. Geological Society of London, Special Publication no. 272.

ŞENGÖR, A. M. C. 1979. The North Anatolian transform fault: its age, offset and tectonic significance. *Journal of the Geological Society, London* **136**, 269–82.

ŞENGÖR, A. M. C., GÖRÜR, N. & ŞAROĞLU, F. 1985. Strike-slip faulting and related basin formation in zones of tectonic escape: Turkey as a case study. In *Strike-Slip Deformation, Basin Formation and Sedimentation* (eds K. D. Biddle & N. Christie-Blick), pp. 227–64. Society of Economic Paleontologists and Mineralogists, Special Publication no. 17.

ŞENGÖR, A. M. C., TÜYSÜZ, O., İMREN, C., SAKINÇ, M., EYIDOĞAN, H., GÖRÜR, N., LE PICHON, X. & RANGIN, C. 2005. The North Anatolian Fault; a new look. *Annual Review of Earth and Planetary Sciences* **33**, 37–112.

SOSSON, M., ROLLAND, Y., MÜLLER, C., DANELIAN, T., MELKONYAN, R., KEKELIA, S., ADAMIA, S., BABAZADEH, V., KANGARLI, T., AVAGYAN, A., GALOYAN, G. & MOSAR, J. 2010. Subductions, obduction and collision in the Lesser Caucasus (Armenia, Azerbaijan, Georgia), new insights. In *Sedimentary Basin Tectonics from the Black Sea and Caucasus to the Arabian Platform* (eds M. Sosson, N. Kaymakci, R. A. Stephenson, F. Bergerat & V. Starostenko), pp. 329–52. Geological Society of London, Special Publication no. 340.

SPADINI, G., ROBINSON, A. & CLOETINGH, S. 1997. Thermo-mechanical modelling of Black Sea Basin formation, subsidence and sedimentation. In *Regional and Petroleum Geology of the Black Sea and Surrounding Areas* (ed. A. Robinson), pp. 19–38. American Association of Petroleum Geologists, Memoir 68.

STAMPFLI, G. M. & BOREL, G. D. 2004. The TRANSMED transects in space and time: constrains on the paleotectonic evolution of the Mediterranean domain. In *The TRANSMED Atlas – The Mediterranean Region from Crust to Mantle* (eds W. Cavazza, F. Roure, W. Spakman, G. M. Stampfli & P. A. Ziegler), pp. 53–80 (see also Appendix 3). Berlin, Heidelberg: Springer.

TEZCAN, A. K. 1995. Geothermal explorations and heat flow in Turkey. In *Terrestrial Heat Flow and Geothermal Energy in Asia* (eds M. L. Gupta & M. Yamano), pp. 23–42. Rotterdam: Balkema Publishers.

VINCENT, S. J., CARTER, A., LAVRISHCHEV, V. A., RICE, S. P., BARABADZE, T. G. & HOVIUS, N. 2011. The exhumation of the western Greater Caucasus: a thermochronometric study. *Geological Magazine* **148**, 1–21.

VINCENT, S. J., MORTON, A. C., CARTER, A., GIBBS, S. & BARABADZE, T. G. 2007. Oligocene uplift of the Western Greater Caucasus; an effect of initial Arabia-Eurasia collision. *Terra Nova* **19**, 160–6.

YILMAZ, Y. 1993. New evidence and model on the evolution of the southeast Anatolian orogen. *Geological Society of America Bulletin* **105**, 252–71.

YIN, A., DANG, Y.-Q., ZHANG, M., CHEN, X.-H. & MCRIVETTE, M. W. 2008. Cenozoic tectonic evolution of the Qaidam basin and its surrounding regions (Part 3): structural geology, sedimentation, and regional tectonic reconstruction. *Geological Society of America Bulletin* **120**, 847–76.

ZATTIN, M., LANDUZZI, A., PICOTTI, V. & ZUFFA, G. G. 2000. Discriminating between tectonic and sedimentary burial in a foredeep succession, Northern Apennines. *Journal of the Geological Society, London* **157**, 629–33.

ZIEGLER, P. A., CLOETINGH, S. & VAN WEES, J.-D. 1995. Dynamics of intra-plate compressional deformation: the Alpine foreland and other examples. *Tectonophysics* **252**, 7–59.

ZIEGLER, P. A., VAN WEES, J.-D. & CLOETINGH, S. 1998. Mechanical controls on collision-related compressional intraplate deformation. *Tectonophysics* **300**, 103–12.